UPPSALA
UNIVERSITET

ISRN UTH-INGUTB-EX-E-2025/008-SE

Examensarbete 15 hp

Juni, 2025

# Design and Simulation of a Motor Driver for Rotor Speed Synchronization in a CRVT

Oscar Englundh & Moa Silfver

Högskoleingenjörsprogrammet i elektroteknik

UPPSALA
UNIVERSITET

Design and Simulation of a Motor Driver for Rotor Speed Synchronization in a CRVT

Oscar Englundh & Moa Silfver


## Abstract

This thesis presents the design and simulation of a motor driver circuit intended for controlling the rotor speed of a test rig for a Counter Rotating Axial Floating Tilting (CRAFT) wind turbine. Using LTspice, the motor control circuit was developed with Sinusoidal Pulse Width Modulation (SPWM) to regulate an asynchronous motor, while thermal calculations ensured adequate cooling of the IGBT modules in the rectifier. Simulations were conducted at various switching frequencies, slip values, and DC bus voltages to assess motor performance and power losses, successfully demonstrating the motor mode's functionality. However, attempts to simulate the generator mode in LTspice encountered convergence issues due to negative impedance values, highlighting limitations in the software. The study suggests that Simulink, with its predefined induction generator models, might be a more suitable tool for such simulations. Thermal management was addressed through heat sink selection based on maximum thermal resistance calculations, with results indicating that higher switching frequencies are viable within thermal limits. Despite challenges, the project has offered valuable insights into motor driver design for innovative wind turbine systems, while acknowledging mixed outcomes and areas for improvement.


**Faculty of Science and Technology**

**Uppsala University, Place of publication Uppsala**

Supervisor: Izabella Simonsson  Subject reader: Hans Bernhoff

Examiner: Andrej Savin

# Populärvetenskaplig sammanfattning

I denna uppsats undersöks utvecklingen av en motodrivarkrets för en asynkronmaskin i en ny typ av vindturbin som kallas CRAFT. CRAFT är ett flytande vindkraftverk med vertikal axel, designat för att kunna generera en effekt på upp till 40 megawatt. Till skillnad från traditionella vindkraftverk, som oftast är fastmonterade till marken eller havsbotten samt horisontalaxlade, erbjuder CRAFT en mer effektiv lösning som lämpar sig särskilt väl för djupa havsmiljöer där konventionella vindkraftverk inte lämpar sig väl.

Syftet med projektet har varit att designa en drivkrets som reglerar asynkronmaskinens rotationshastighet. För att uppnå detta har styrkretsen tagits fram och simulerats i simuleringsprogrammet LTspice. Kretsen utgörs av en trefas växelriktare som använder sig av sinusformad pulsbreddsmodulering (SPWM), en metod som möjliggör styrningen av rotationshastigheten.

En viktig aspekt av arbetet har varit att säkerställa att den elektroniska utrustningen inte överhettas vid drift. Därför har termiska beräkningar genomförts för att fastställa vilken maximal termisk resistans som systemets kylfläns får ha. Resultaten från dessa beräkningar har legat till grund för valet av en lämplig kylfläns. Kylflänsen är nödvändig för att kunna garantera en säker och stabil temperaturreglering av elektroniken även vid höga effektförluster.

Under projektet uppstod flera tekniska utmaningar. Särskilt komplicerat visade sig simuleringen av asynkronmaskinen i generatorläget vara, där vissa begränsningar i LTspice blev uppenbara. Detta ledde till diskussioner om alternativa lösningar, som att använda andra simuleringsverktyg. Trots dessa hinder har projektet givit värdefulla insikter om praktiska och teoretiska aspekter av styrkretsdesign i moderna vindkraftsystem. Utvecklingen av vindkraft utgör ett steg mot en mer tillförlitlig, energieffektiv och hållbar energiproduktion som behövs för att motverka klimatförändringar.

# Contents

# 1 Introduction

## 1.1 The Evolution of Wind Turbines

The first known windmill was put to use in Persia in the year 644 A.D. and was a vertical axis wind turbine (VAWT) called Sistan windmill. Initially, wind turbines were used to grind grains and pump water. It was not until the 12th century that windmills were operated in the north of Europe. The European windmills were proved to be useful in areas such as farming and forestry.

In 1888, the very first automatically operated, power-generating wind turbine was invented in Ohio, USA by Charles F. Brush and could generate 12 kW. The HAWT had a rotor with a diameter of 17.1 metres and consisted of 144 thin strips of wood. His invention is depicted in figure 1.

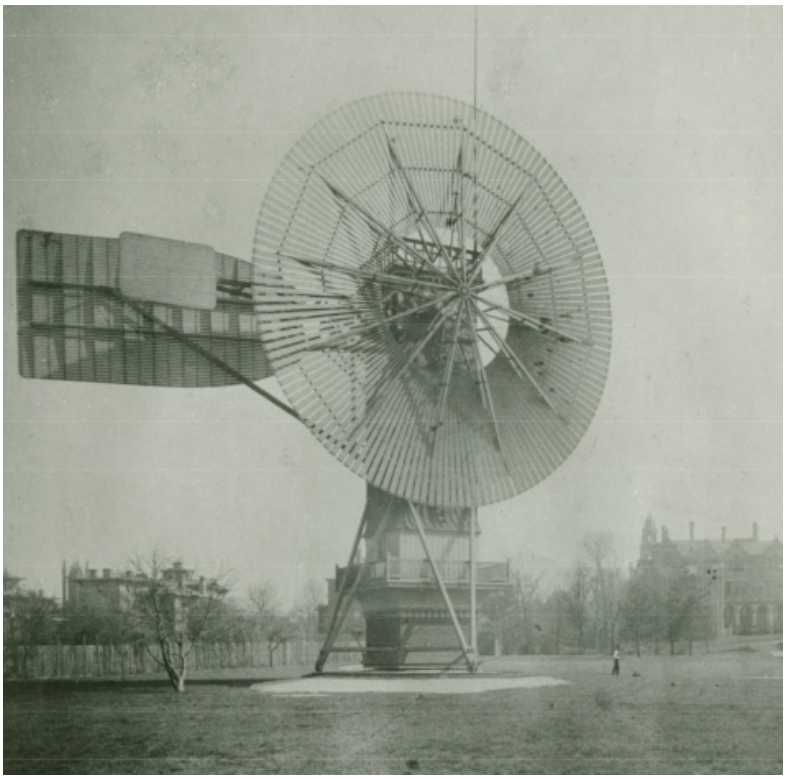

Figure 1: Charles F. Brush's wind turbine from 1888 - the first automatically operated, electricity-generating wind turbine. The horizontal-axis wind turbine featured a pilot vane for control of the wind direction.

In the very end of the 1800s, the Danish inventor, teacher and meteorologist Poul la Cour started to look into wind power, which is what he would later come to be best

known for. At this point in time, coal-burning was being introduced as a power-source in Denmark. With his meteorological background, La Cour was convinced that it would be in Denmark's best interest to harvest the large amounts of wind energy that were present instead of burning the small supply of coal that Denmark had at hand. He would come to design over 100 power-generating wind turbines with the capacity of between 20 and 35 kW. The construction of his HAWTs was inspired by Danish smock mills. La Cour experimented on different designs of turbines and came to the conclusion that turbines with fewer blades and faster rotation speed were more efficient than slow wind turbines with many rotor blades, which came to pave the way for further wind power development.

Until 1919, the wind turbines were solely used to provide direct current (DC) for small villages - often via batteries. Following the end of world war I, a wind turbine called Agricco, with a capacity of 40kW was interconnected with an alternating current (AC) network for the first time. To enable grid-connection, an induction generator was used inside of a wind turbine, which was a new technique for this point in time. The Agricco can be seen in Figure 2.

Following world war II, a former student of Poul la Cour by the name of Johannes Juul began experimenting on different types of wind turbines. He designed two wind turbines which incorporated attributes still used to this day - for instance he concluded that three rotor blades was the most efficient design choice. Juul turned the nacelle of the wind turbines towards the wind, which was new for that time. He also introduced pitchable blade tips, which was a new technique to control the rotational speed of the rotor blades and limit the generated power in order to protect the induction generator from overloading. Before this point, stall regulation was the only existing technique. In the case of stall regulation, the rotor blades are fixed and automatically slow the rotational speed down by moderately increasing the wind's angle of attack and thus decreasing the lift force of the blade. Juul acknowledged the disadvantages of stall regulation; it would not work if the generator would be overloaded and the turbine could potentially spin uncontrollably fast leading to destruction. On the contrary, the pitchable blade tips allow the rotational speed of the turbine to decrease by shifting the blade's angle relative to the airflow [1],[2].

## 1.2 Advantages of offshore wind power

Climate change has sparked the ongoing aim for a future with solely green energy production, and wind power is at the top among the most rapidly increasing renewable energy sources. Currently, the majority of wind power is harvested on land but benefits related to offshore energy have lead to an increasing amount of offshore wind farms worldwide since the mid 1990's when the first one was set in the works. In 2023, global wind power production reached a total of 1025 gigawatts. Out of this, 7% came from

Figure 2: The Agricco wind turbine - the first to be connected to an AC grid.

offshore installations. Onshore wind, having been adopted widely, is now present in 115 countries. On the contrary, offshore wind power is currently used in 21 nations, making it far less widespread. In 2023, a total of 116 gigawatts of new wind power was installed worldwide, and out of this, 9% originated from new offshore wind farms being installed. Offshore technology is expected to expand further in the future as policies in the united states and european union have been changed in order to allow for more offshore wind farms to be installed [3].

Offshore wind turbines can be placed either at sea or in lakes. Offshore wind farms free up space on land for farming and the construction of new residential areas. More often than not, the strength and steadiness of the winds longer out at sea are stronger than those on or closer to land, causing more constant energy production [4]. Approximately 80% of offshore wind is at deep sea levels. In order to harvest this wind, floating wind

turbines is a requirement as it quickly becomes more complicated and expensive to mount wind turbines to the sea bed as the water depth increases [5].

## 1.3 CRAFT

Counter Rotating Axial Floating Tilting wind turbine (CRAFT) is an innovative offshore turbine currently in development. The CRAFT is a CRVT (Counter- rotating vertical axis turbine) which is a new type of turbine that builds upon the design of the VAWT. The design allows for the generator to be positioned at the base of the tower, which provides stability [6]. Traditionally designed offshore HAWTs produced in the early 2020s typically achieve a maximum power output of approximately 10-15 MW per turbine [7]. In contrast, the CRAFT is designed to generate up to 40 MW, significantly improving the potential of power production.

The CRAFT is a direct drive turbine which means that the rotor is directly connected to the generator. Thus, there is no need for a gearbox. The design causes less wake than traditional HAWTs which enables for the turbines to be placed closer to one another which doubles the possible number of turbines within a certain water area [5].

The CRAFT consists of two turbines, each with three rotor blades mounted on a spar buoy for stability. The wind turbine is equipped with two separate generators: the primary generator, where the rotor is driven by the upper turbine and the stator by the lower turbine, and the secondary generator, where the rotor is connected to the upper turbine while its stator remains fixed. The generators are housed in a dry compartment below the water level, where they act as ballast, further improving stability. Unlike conventional wind turbines, the CRAFT uses a counter-rotating system in which one turbine drives the rotor of the primary generator in one direction while the other set of rotor blades drives the stator of the primary generator in the opposite direction. This configuration not only increases power generation, but also helps reduce the torque load on the primary generator [8]. The different parts of the CRAFT can be seen in Figure 3.

One potential challenge with this counter-rotating design is the difference in wind speed between the upper and lower turbine. If not managed, this could cause the lower turbine to stop while the upper turbine accelerates beyond safe operational limits. To counteract this issue, the system incorporates a secondary generator capable of functioning as a motor [6].

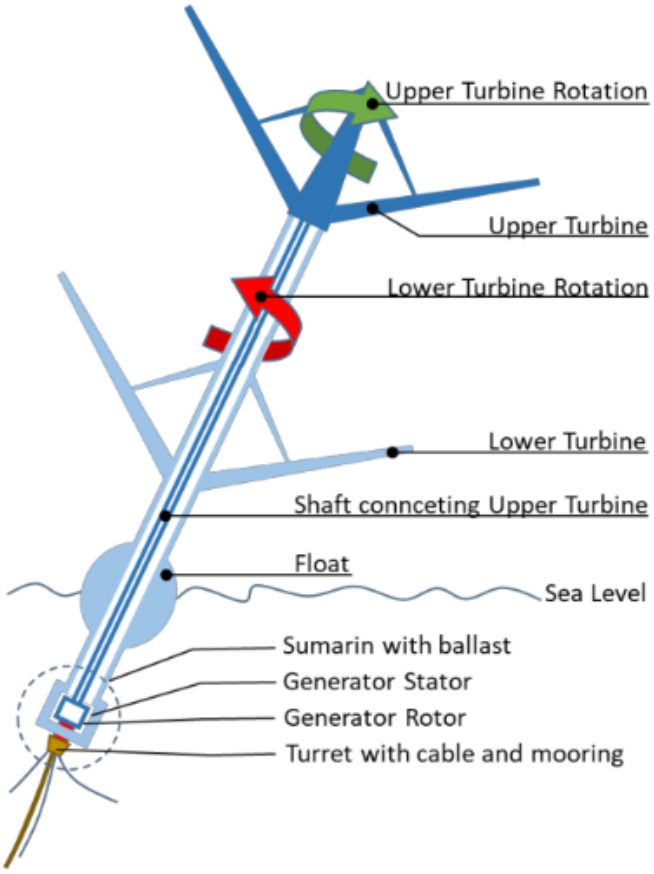


Figure 3: An illustration of the CRAFT wind turbine

The electrical system is presented in figure 4. The upper wind turbine is connected to the primary generator, which is a permanent magnet synchronous generator (PMSG). The turbine converts wind energy into mechanical energy, and in turn, the primary generator converts the mechanical energy into 3-phase AC power. The turbine and primary generator are regulated using maximum power point tracking (MPPT). MPPT technology is used to ensure that the turbine operates at its most efficient point on the power curve, which maximizes energy capture [9]. The resulting three phases are then connected to a 6-diode rectifier which converts the AC power to DC power. Following, a boost converter is used to increase the voltage to an acceptable level.

The lower wind turbine is connected to a secondary generator which is an asynchronous generator. Just like with the primary generator, the turbine converts wind energy into

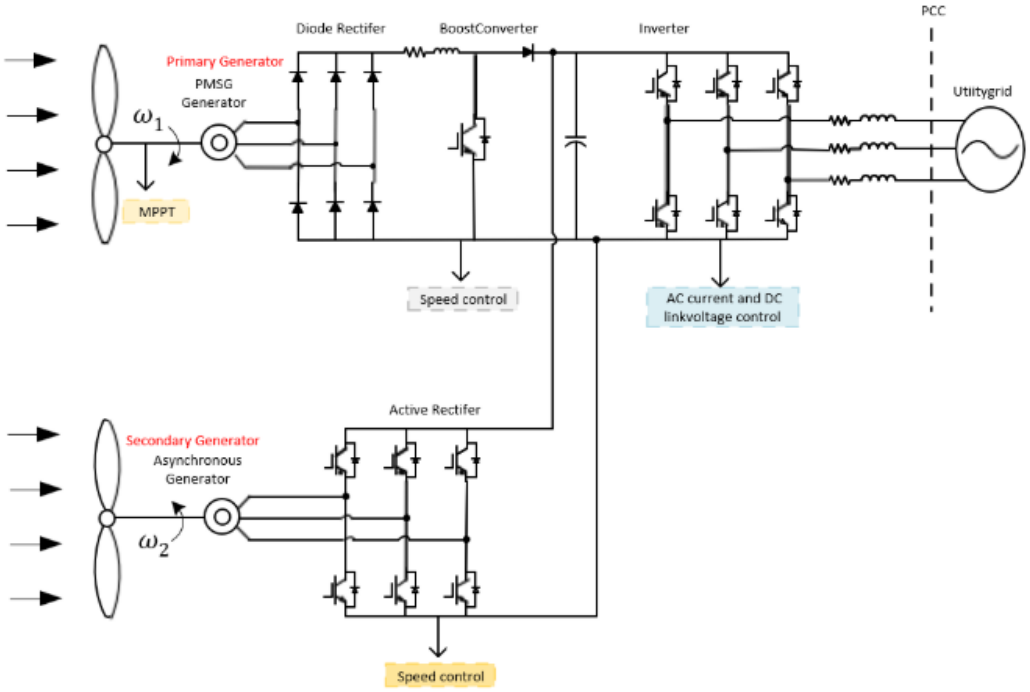


Figure 4: Overview of the electrical system of the CRAFT wind turbine

mechanical energy, and in turn, the secondary generator converts the mechanical energy into 3-phase AC power. The secondary generator is controlled by a motor driver circuit, consisting of an active rectifier constructed by six insulated gate bipolar transistors (IGBTs), which enables it to act bidirectionally; as a generator or motor depending on what the system needs. By usage of an automatic control system the rotation speed of the secondary turbine can managed. The automaic control system will not be discussed further in this report as the main focus of this thesis is the operational functionality of the driver circuit.

One side of the active rectifier is connected to the output of the boost converter and the other side is connected to a smoothing capacitor which reduces the ripples of the voltage. The smoothing capacitor is connected to an IGBT inverter which transforms the DC power to AC power which is phase-balanced with the grid.

## 1.4 The asynchronous generator

The asynchronous generator is also known as an induction generator. It is a rotating electrical machine made to convert mechanical energy into electricity.

Unlike the synchronous generator, the asynchronous generator's stator has a difference in rotational speed in comparison to the synchronous speed. This difference is called slip. The synchronous speed is defined as the rotational speed of the magnetic field which is present inside of the stator. The rotational speed of the magnetic field depends on the number of poles as well as the frequency. In the asynchronous generator, the rotor rotates faster than the magnetic field, leading to a negative slip-value. In generator mode the induction generator transforms mechanical energy into electrical power. If the rotor is rotating slower than the magnetic field, the slip value will become positive. This will cause the machine to go into motor-mode and thus convert electrical energy into mechanical energy. In other words, the function of the asynchronous machine can be controlled by adjusting the slip, which is achieved by controlling the rotational speed of the rotor, which is dependent on the frequency. This characteristic is depicted in figure 5.

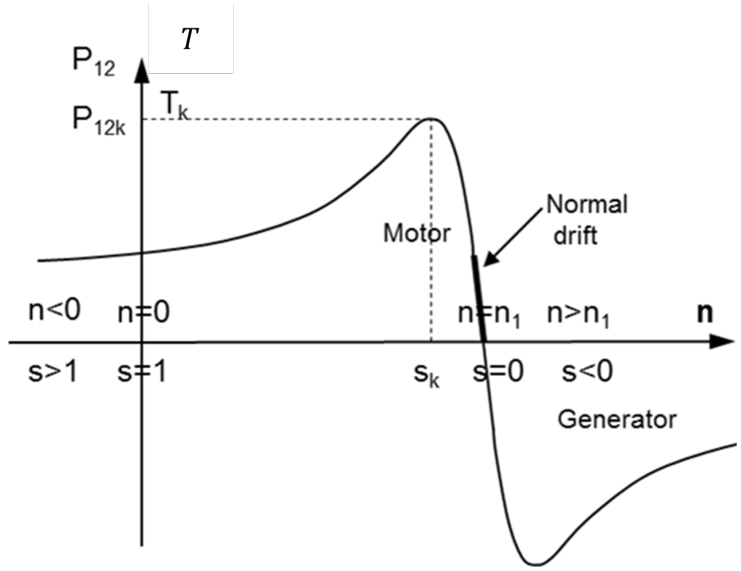


Figure 5: Torque and power as a function of speed or slip for a typical asynchronous machine.

When an AC power supply is applied, it generates a rotating magnetic field around the stator. The difference in speed between this magnetic field and the stationary rotor conductors induces an electromagnetic field within the rotor due to electromagnetic induction. As a result, electric current is produced in the rotor, generating an alternating

magnetic flux. This rotor flux lags behind the stator's rotating field but moves in the same direction, continually trying to reach synchronous speed, though it never fully does.

Induction motors are widely used due to their attributes. One of their main advantages is that they are self-starting, requiring no external excitation to begin operation. As load increases, the motor's speed slightly decreases; a natural behavior caused by the slip between the rotating magnetic field and the rotor. These motors perform well at higher speeds, making them ideal for many industrial applications.

In contrast, synchronous motors operate at a constant speed regardless of load but are not self-starting. They require an external DC power source to initiate motion and often include damper windings to provide the torque needed during startup [10].

## 1.5 Three Phase Bridge Rectifier

The asynchronous generator is connected to a three phase active rectifier. The rectifier's task is to convert three phase alternating current into direct current. The rectifier uses six insulated-gate bipolar transistors (IGBTs) as switches, which enables control of the switching frequency as opposed to using a diode rectifier.

The switches are connected in a bridge layout. Each one of the three phases is connected to a series connection of two IGBTs. This creates a "high side" and a "low side" in each phase. Each one of the IGBTs is switching between being ON and OFF in order to manage the current flow. The IGBT on the high side is switched on when its phase voltage is positive, while the low side IGBT is turned off. Conversely, a negative phase voltage turns the IGBT on the low side on and the high side IGBT gets switched off. When the high-side switch is on it is forward-biased, which means it allows current to flow through the switch and the load. When the low-side switch is turned on, current will flow through the load but in the opposite direction. The rectifier configuration allows for bidirectional power flow [11].

## 1.6 Purpose

The goal of this thesis is to create a SPICE simulation of a bidirectional motor driver circuit for the asynchronous motor in the test rig of a CRAFT. Calculations will also be made in order to determine appropriate temperature management of the driver circuit.

## 1.7 Main research questions

- How can the bidirectional motor driver circuit be designed?
- How large will the power losses be when employing the design?
- Which method is suitable in terms of thermal management of the motor driver circuit?

## 1.8 Delimitations

The main focus of this work will be the temperature management as well as the design of the motor drive circuit which controls the asynchronous generator. This includes design choices regarding electrical components and their configuration. Pregiven parameters for the asynchronous generator will be taken into account in the making of design choices. The thesis will not include discussion of other topics.

# 2 Theory

## 2.1 LTspice

LTspice is a SPICE (Simulation Program with Integrated Circuit Emphasis) software provided by Analog Devices, initially developed by Linear Technologies. LTspice is primarily made for simulating analog electronics. The simulation of integrated circuits before their construction is crucial to avoid additional costs and delays caused by errors made in the design process.

SPICE is a programming language that needs to be interpreted by a SPICE interpreter - like LTspice. The circuits described in LTspice can be entered in the program either by drawing a schematic or by entering SDL (spice description language) in a source file - also called netlist. In the netlist the user can enter attributes for electrical components and their connections as well as what sort of analysis that should be executed. Then, the circuit descriptions can be processed through calculations based on nonlinear algebraic equations by applying various numerical methods [12] [13].

SPICE software can also be used to simulate thermal and mechanical systems. As electrical, thermal, and mechanical systems are governed by equations of the same form the different units can be substituted for others [14][15]. Some examples of analogous properties are shown in Table 1.

Table 1: Electrical to Thermal Analogy.

| Thermal | Electrical |
|---|---|
| Power ($W$) | Current ($A$) |
| Temperature ($^{\circ}C$) | Voltage ($V$) |
| Thermal Resistance ($K/W$) | Resistance ($\Omega$) |
| Thermal Capacitance | Capacitance ($F$) |

Using these relationships it is possible to set up a SPICE program to simulate the thermal properties of a system and calculate temperatures, for example the junction temperature of an IGBT in an inverter circuit.

## 2.2 Equivalent circuit of the induction motor

The induction motor can be modeled as a simplified one phase circuit equivalent. This can be seen in Figure 6 where $s$ is the slip of the machine, $R_0$ is the stator resistance, $X_0$ is the stator inductance while $X_2'$ and $R_2'$ correspond to the rotor inductance and rotor resistance, respectively. Connecting three one phase equivalents in a delta connection allows for simulation of a complete three phase motor equivalent [10].

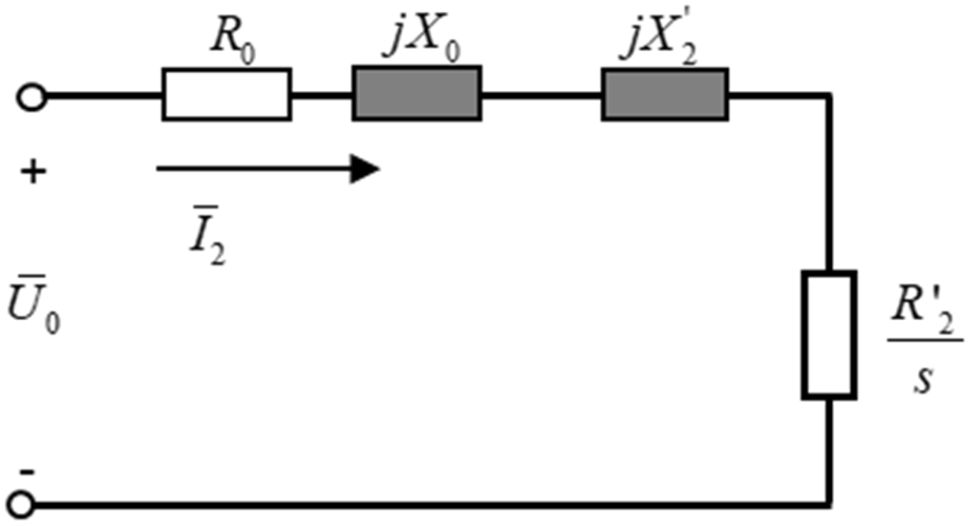


Figure 6: Simplified circuit equivalent of the induction motor

## 2.3 Thermal management

Due to power losses in the IGBT modules, measures need to be taken in order to protect the electronics from overheating as this would result in system failure. In IGBTs there are two main categories of losses: switching losses and conduction losses. Conduction losses occur during the on-state according to the voltage drop across the IGBT and the conducted current. Switching losses happen when the IGBT switches between the on-state and off-state and vary based on the cycle duration, the switching speed, current and switching voltage. As the switching losses are tied to the switching frequency one can adjust these losses by changing the frequency.

In order to determine which heat sink to choose for thermal management, one first has to calculate the heat sink's maximal allowed thermal resistance to meet the IGBT modules thermal requirements. This is calculated using the equation below.

$$R_{th-ha} = \frac{(T_{heatsink} - T_a)}{P} \tag{1}$$

Where $R_{\text{th-ha}}$ is the maximum required thermal resistance from the heat sink to ambient, $P$ is the power dissipation per IGBT, $T_a$ is the ambient temperature temperature, $T_{\text{heatsink}}$ is the temperature of the heatsink [16].

# 3 Implementation

## 3.1 Control of the induction motor by using SPWM

In the LTspice simulations made, the induction motor is controlled by three phase Sinusoidal Pulse Width Modulation (SPWM). This is carried out by - for each of the six IGBTs - comparing a sinusoidal reference waveform with a triangular carrier waveform. By employing an if-statement in the component attribute editor window for the variable voltage source of each phase, the PWM signal is defined. For each time instant, the if-statement examines whether the magnitude of the sinusoidal waveform is bigger or smaller than the carrier waveform. For the high side switches; if the value of the sinusoidal waveform is smaller than the carrier waveform, the PWM-signal will be in high level and if it is smaller it will be in low level. The PWM-signal goes from one level to the other when the reference signal and the carrier signals intersect.

## 3.2 Simulation of the induction motor

In order to simulate the induction motor in LTspice, three one phase equivalent circuits (as depicted in Figure 6) were connected in a delta-configuration. In this project the motor parameters were taken from research done by staff at the department of electrical engineering at Uppsala University. For this reason, the derivation of the motor parameters will not be included in this report.

The motor design used in the simulations is a 12-pole induction motor with $R_0 = 0.07118\Omega$, $X_0 = 6.304mH$, $X_2' = 10.05mH$, and $R_2' = 0.162\Omega$. It is designed to run at 20rpm, 50kW at a slip of between 2% and 3%.

## 3.3 The IGBT model

The IGBTs used in the simulation were chosen to be FF600R12KT4 from Infineon. This model was chosen because it matched the preliminary requirements given in the beginning of the project. Infineon does not supply a SPICE model for this IGBT module, so the IKY75N120CH3 was chosen as a substitute according to manufacturer recommendations. This was done by using eight IKY75N120CH3 in parallel to simulate each FF600R12KT4 [17].

# 4 Results

Table 2: Simulation results of the induction motor at 20 rpm for different switching frequencies, slip values and DC bus voltage values.

| Slip (%) | $F_{sw}$ (kHz) | $V_{bus}$ (V) | $Power_{motor}$ (kW) | $Losses$ (W) |
|---|---|---|---|---|
| 1.0 | 1 | 600 | 24.564 | 104.673 |
| 2.0 | 1 | 600 | 48.394 | 238.201 |
| 3.0 | 1 | 600 | 71.032 | 381.263 |
| 0.5 | 5 | 600 | 12.287 | 58.304 |
| 1.0 | 5 | 600 | 24.358 | 126.828 |
| 1.5 | 5 | 600 | 36.241 | 201.074 |
| 2.0 | 5 | 600 | 47.986 | 279.106 |
| 2.5 | 5 | 600 | 59.511 | 361.472 |
| 3.0 | 5 | 600 | 70.850 | 447.584 |
| 2.0 | 10 | 600 | 47.849 | 333.017 |
| 3.0 | 10 | 600 | 70.517 | 530.691 |
| 2.0 | 5 | 500 | 33.277 | 217.107 |
| 3.0 | 5 | 500 | 49.132 | 346.489 |

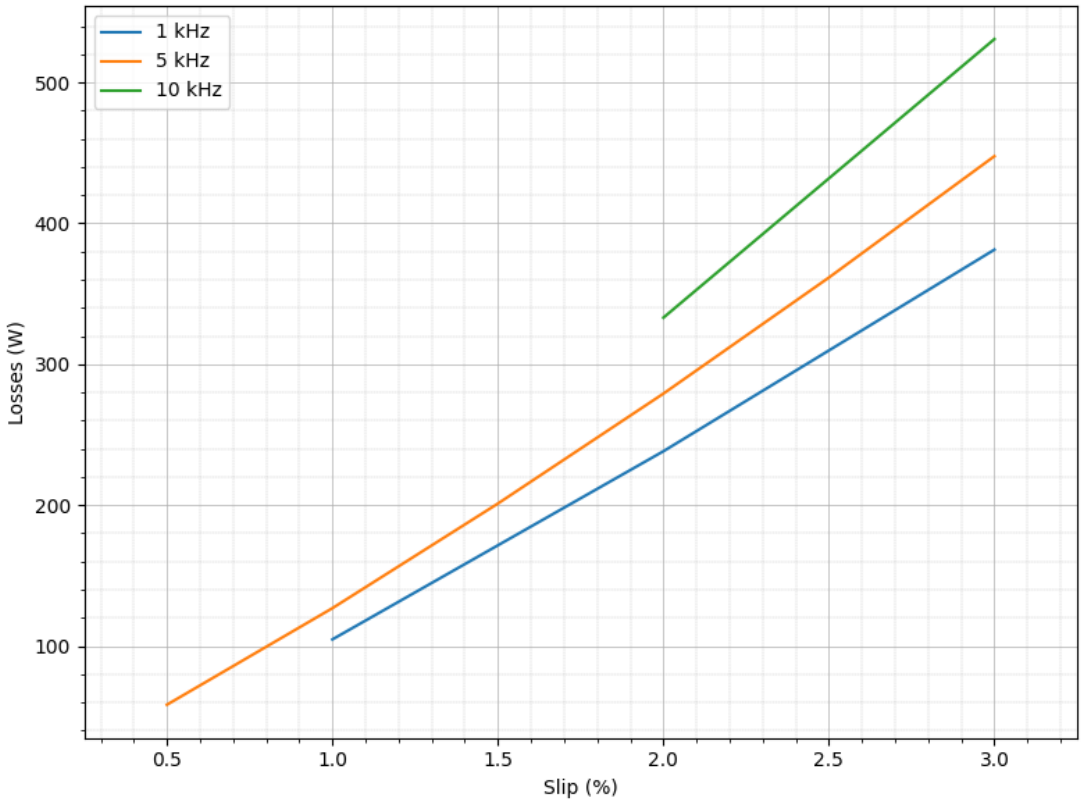


Figure 7: Power losses plotted against slip for the three simulated frequencies with $V_{bus} = 600V$

## 4.1 Thermal calculations

The losses are evenly distributed across all IGBTs, with a maximum difference of less than $1W$ between each IGBT. For the thermal calculations the power $P$ in each IGBT is therefore set to one sixth of the total losses, rounded up to the nearest half watt. Using the values in Table 2 and the method described in Section 2 we can calculate the maximum allowed thermal resistance of the heat sink. Selecting the situation with the highest losses, 3% slip at 10 kHz, we get $P = 88.5W$ and use the following values taken from the datasheet of the IGBT:

$$R_{\text{th-jc}} = 0.046K/W$$
$$R_{\text{th-ch}} = 0.0226K/W$$
$$T_j = 150°C$$

$$T_a = 25°C$$

The temperature delta from junction to case then becomes:

$$T_{jc} = R_{\text{th-jc}} * P = 0.046K/W * 88.5W = 4.071K \tag{2}$$

The temperature delta from case to heat sink becomes:

$$T_{ch} = R_{\text{th-ch}} * (2 * P) = 0.0226K/W * (2 * 88.5W) = 4.0002K \tag{3}$$

Using these values we can calculate the maximum allowed temperature of the heat sink:

$$T_{heatsink} = T_j - T_{jc} - T_{ch} = 150°C - 4.071K - 4.0002K = 141.9288°C \tag{4}$$

Now we can calculate the maximum allowed thermal resistance of the heat sink:

$$R_{th-ha} = \frac{(T_{heatsink} - T_a)}{6 * P} = \frac{141.9288°C - 25°C}{6 * 88.5W} = 0.220204896K/W \tag{5}$$

## 4.2 Heat sink selection

The selected heat sink needs to have a thermal resistance lower than that calculated in the previous section. It also needs to be large enough to fit the IGBT modules, each of which is 62mm by 107mm. Placing three modules side by side requires an area of at least 186mm by 107mm. Using these criteria, the model LA 7 200 12 from Fischer Elektronik is selected [18]. It is large enough to fit all three modules with room to spare and has a thermal resistance of around $0.075K/W$, almost three times better than what is required.

Opting for an oversized heat sink accommodates potential calculation inaccuracies and unforeseen variables. This choice ensures robust thermal management, enhancing the reliability and longevity of the IGBT modules under varying operational conditions.

By creating a simulation as explained in Section 2.1 the junction temperature of the IGBTs can be calculated. Using the thermal resistance of the selected heat sink the temperature rise of the IGBTs is found to be $48°C$. At an ambient temperature of $25°C$ this gives a maximum junction temperature of $73°C$, well within the limit of the IGBTs which is $150°C$.

# 5 Discussion

## 5.1 Selection of switching frequency

Selecting the switching frequency is an exercise in compromise. A higher switching frequency causes fewer potential issues and stresses for the mechanical parts of the system but increases the stresses on the electrical parts of the system. Therefore a "sweet spot" has to be found, where these aspects are balanced. Simulations were made at three different frequencies: 1 kHz, 5 kHz, and 10 kHz. At 1 kHz the current ripple becomes very large and as such it is not considered suitable for actual usage. The Frequencies 5 kHz and 10 kHz have a lot smaller current ripple, with 10 kHz having the least. Most simulations were done at 5 kHz in an attempt to increase the simulation speed as 10 kHz doubles the time needed. As the differences in motor power between 5 kHz and 10 kHz are minute this was considered an acceptable tradeoff. Even higher frequencies might be suitable and possible if needed, especially as the thermal limits are far from reached.

The effects on the power losses from switching frequency are quite apparent when looking at Table 2. Assuming that the losses for each switching event are constant then only the switching losses will change when varying the frequency. By fitting the results for 1 kHz, 5 kHz, and 10 kHz at 3% slip, 600V, to a curve the conduction losses and the switching losses can be found and also approximated for higher frequencies. The equation then becomes:

$$P_{loss} = 0.0166 * F_{sw} + 364.6 \tag{6}$$

where $P_{loss}$ is the power loss in watts, and $F_{sw}$ is the switching frequency in Hz. Applying this equation for a switching frequency of 20 kHz results in a power loss of $696.6W$ and for 40 kHz the power loss is $1028.6W$.

By applying the simulation method described in Section 2.1 the calculated losses can be simulated and the junction temperature can be calculated. This gives $T_j = 87.8°C$ for $F_{sw} = 20kHz$ and $T_j = 117.8°C$ for $F_{sw} = 40kHz$ with $T_a = 25°C$.

## 5.2 Selection of bus voltage

The bus voltage was chosen in concert with the thesis supervisor and the subject reviewer according to calculations done by them. During the simulations it appeared that the voltage was too high as the power in the motor was higher than expected, reaching almost 71kW at 3% slip. Lowering the voltage from 600V to 500V reduced the motor power to 49kW at 3% slip. Depending on the desired slip the bus voltage should therefore be in the range of 500V to 600V.

## 5.3 SPICE issues

The LTspice model for the IGBT (IKY75N120CH3) exhibited numerical convergence issues under certain operating conditions, particularly at high slip values. This was mitigated by setting the $gshunt$ parameter to 1e-12, adding minimal conductance to stabilize the solver. Furthermore, the complexity of the model significantly reduced the computational efficiency, limiting simulations to approximately two per day. Adjusting tolerances ($abstol$ (absolute current error tolerance) to 1e-11, $reltol$ (relative error tolerance) to 0.01, $vntol$ (absolute voltage error tolerance) to 1e-5 improved simulation speed with minimal impact on precision, highlighting the need for optimized models in future studies.

The slow simulations were a major hindrance to the project as changes to the models could not be quickly checked. Only about two complete simulations could be run per day. Replacing the IGBT models with simple switch models and diodes allowed changes to the motor model and circuit connections to be simulated a lot quicker, allowing for faster iteration. Sadly these simple switch models are a poor substitute for the real IGBT models when it comes to accuracy, especially when it comes to power losses in the IGBTs.

While using another software like Simulink for the motor and generator simulations would have been a large improvement over what was used, it would not solve the issues with the IGBT models. Having searched for other IGBT models it was found that most are either not very accurate or are very slow, like the one that was used in this project.

## 5.4 Generator issues

This project was initially supposed to create a model of an induction machine working in both motor and generator mode. But due to issues with creating a working SPICE model for the generator model, this part had to be removed from the project. The standard equivalent circuit model for an induction motor, when adapted for generator mode with negative slip, introduces a negative resistance in the rotor branch. This leads to numerical instability in SPICE, as the solver cannot handle the resulting negative impedance, causing the current to diverge. Attempts to stabilize the model by adjusting circuit parameters or employing alternative representations, as suggested by Watson [19], were unsuccessful due to persistent convergence issues.

The limitations of LTspice in modeling the induction generator suggest that alternative simulation tools may be better suited for this application. MATLAB/Simulink, for instance, offers predefined libraries within Simscape Electrical that include robust models for induction machines operating in both motor and generator modes. These models account for dynamic interactions between electrical and mechanical domains, which

are critical for accurately simulating the counter-rotating turbines of the CRAFT. Unlike SPICE, which struggles with negative impedances, Simulink's numerical solvers are designed to handle such complexities, potentially resolving the convergence issues encountered in this study.

## 5.5 Improved motor model

It would have been possible to create an improved motor model that includes parameters such as torque or even mechanical losses using the methods described in Section 2.1. Such a model would be a lot more complex than the simple model used in this study, making it possible that it would bring its own share of problems. However, it would nonetheless bring a lot of possibilities for more complex and useful simulations using SPICE.

# 6 Conclusions

In hindsight, it would have been more suitable to use another software for the simulations in this project. Simulink, which is made for multi-domain simulations of dynamical systems, might have been a better option as it has add-on libraries where a model of the induction generator is already available. This would likely have solved the occurring problems (described in 5.4) when attempting to simulate the induction generator. However, due to the project's time constraints, this was not considered an appropriate option, as learning to operate new software would have been significantly more time-consuming compared to using a familiar simulation tool. Although the simulation of the generator mode fell flat, the power losses of the IGBTs would have been the same regardless of the direction of the motor driver.

The simulations revealed that among the three switching frequencies tested, 10 kHz proved to be the most suitable when it came to balancing the performance of the motor while minimizing the power losses. To further examine this and possibly make further improvements, it would be beneficial to perform additional simulations at a wider range of switching frequencies. Simple calculations show that even higher switching frequencies are possible while comfortably staying within the thermal budget.

This project shows that it is possible to simulate an induction motor in LTspice and connect it to an electrical system for the evaluation of that system. As a whole this thesis work was a mixture of failures and successes, with several parts having to be changed or even dropped altogether, while other parts worked as expected. This project also shows the viability of using free and sometimes open-source SPICE software for quite complex simulations, while also highlighting some of the drawbacks.

# 7 Acknowledgments

Finally, we would like to express our gratitude for the support and guidance we have received throughout this project from our thesis supervisor Izabella Simonsson and our subject reviewer Hans Bernhoff.

# References


[1] P. Gipe and E. Möllerström, "An overview of the history of wind turbine development: Part i—the early wind turbines until the 1960s," *Wind Engineering*, Aug. 2022. DOI: 10.1177/0309524X221117825.

[2] E. Muljadi, K. Pierce, and P. Migliore, "Control strategy for variable-speed, stall-regulated wind turbines," in *Proceedings of the 1998 American Control Conference. ACC (IEEE Cat. No.98CH36207)*, vol. 3, 1998, 1710–1714 vol.3. DOI: 10.1109/ACC.1998.707298.

[3] P. Bojek. "Wind," The International Energy Agency (IEA). (Feb. 2025), [Online]. Available: https://www.iea.org/energy-system/renewables/wind (Accessed: May 27, 2025).

[4] C. M. Wang, T. Utsunomiya, S. C. Wee and S. C. Choo, "Research on floating wind turbines: a literature survey," *The IES Journal Part a Civil I& Structural Engineering*, vol. 3, no. 4, Oct. 2010. DOI: 10.1080/19373260.2010.517395. [Online]. Available: https://www.tandfonline.com/doi/epdf/10.1080/19373260.2010.517395.

[5] World Wide Wind. "Harnessing the power of nature," [Online]. Available: https://worldwidewind.no/pages/technology (Accessed: May 27, 2025).

[6] I. Simonsson, S. Eriksson and H. Bernhoff, "Design and simulation study of 40 mw pm generator for the craft," *Journal of Physics Conference Series*, Oct. 2023. DOI: 10.1088/1742-6596/2626/1/012010. [Online]. Available: https://iopscience.iop.org/article/10.1088/1742-6596/2626/1/012010.

[7] A. Lejestrand. "Havsbaserad vindkraft." (Apr. 2023), [Online]. Available: https://www.energiforetagen.se/energifakta/elsystemet/produktion/vindkraft/havsbaserad-vindkraft/ (Accessed: May 27, 2025).

[8] H. P. Benjamin and L. Goude, "Dynamics of a craft: A simulation study on a counter rotating vertical axis floating tilting wind turbine," *DIVA*, 2023.

[9] H. Feraoun, M. Fazilat, R. Dermouche, S. Bentouba, M. Tadjine, and N. Zioui, "Quantum maximum power point tracking (qmppt) for optimal solar energy extraction," *Systems and Soft Computing*, vol. 6, Dec. 2024. DOI: 10.1016/j.sasc.2024.200118. [Online]. Available: https://www.sciencedirect.com/science/article/pii/S2772941924000474.

[10] H.Bernhoff, *Roterande Elektriska Maskiner*, 2023.

[11] NEVSemi. "Igbt rectifier: All you want to know - nevsemi electronics." (Aug. 2023), [Online]. Available: https://www.nevsemi.com/blog/igbt-rectifier (Accessed: May 27, 2025).

[12] T. R. Kuphaldt, *Lessons in electric circuits*, Nov. 2021, ch. 7. Using the spice circuit simulation program. [Online]. Available: https://www.ibiblio.org/kuphaldt/electricCircuits/.

[13] *Ltspice*, Analog Devices, 2025. [Online]. Available: https://www.analog.com/en/resources/design-tools-and-calculators/ltspice-simulator.html (Accessed: May 27, 2025).

[14] E. Cheever. "Analogous electrical and mechanical systems," [Online]. Available: https://lpsa.swarthmore.edu/Analogs/ElectricalMechanicalAnalogs.html (Accessed: Jun. 7, 2025).

[15] T. L. Anthony Pham Elizabeth Higgins, *Using pspice simulator to model thermal behavior in ti's smart high-side switches*, 2020-11. [Online]. Available: https://www.ti.com/lit/an/slvaez0/slvaez0.pdf.

[16] C. Qian *et al.*, "Thermal management on igbt power electronic devices and modules," *IEEE Access*, vol. 6, 2018. DOI: 10.1109/ACCESS.2018.2793300.

[17] "Ff600r12kt4 spice model," Infineon. (Sep. 2022), [Online]. Available: https://community.infineon.com/t5/IGBT/FF600R12KT4-Spice-Model/m-p/371491 (Accessed: May 27, 2025).

[18] Fischer Elektronik. "La 7 200 12," [Online]. Available: https://www.fischerelektronik.de/web_fischer/en_GB/heatsinks/D04/Cooling%20aggregates%20with%20axial%20fan/VA/LA720012/index.xhtml (Accessed: Jun. 5, 2025).

[19] D. B. WATSON, "Circuit model and self-excitation of the induction generator," *International Journal of Electrical Engineering & Education*, 1988. DOI: 10.1177/002072098802500219.

# Appendix A Motor SPICE model

```
.subckt MOTOR_MODEL A B C N
.params Rs=0.07118 Rr=0.162 Ls=6.304m Lr=10.05m s=0.03
;Equivalent circuits in delta connection
;Changing the Rxs nodes from B, C, A to N allows for wye-connection
RA1 A NodeA1 {Rs}
LA1 NodeA1 NodeA2 {Ls}
RA2 NodeA2 NodeA3 {Rr}
LA2 NodeA3 NodeA4 {Lr}
RAs NodeA4 B {Rr / s}

RB1 B NodeB1 {Rs}
LB1 NodeB1 NodeB2 {Ls}
RB2 NodeB2 NodeB3 {Rr}
LB2 NodeB3 NodeB4 {Lr}
RBs NodeB4 C {Rr / s}

RC1 C NodeC1 {Rs}
LC1 NodeC1 NodeC2 {Ls}
RC2 NodeC2 NodeC3 {Rr}
LC2 NodeC3 NodeC4 {Lr}
RCs NodeC4 A {Rr / s}

.ends MOTOR_MODEL
```

# Appendix B Motor LTspice symbol

```
Version 4
SymbolType BLOCK
RECTANGLE Normal 48 64 -48 -64
SYMATTR Prefix X
SYMATTR ModelFile Motor.sub
SYMATTR Value MOTOR_MODEL
SYMATTR Value2 Rs=1 Rr=1 Ls=10m Lr=10m s=0.01
PIN -48 -48 LEFT 8
PINATTR PinName A
PINATTR SpiceOrder 1
PIN -48 -16 LEFT 8
PINATTR PinName B
PINATTR SpiceOrder 2
PIN -48 16 LEFT 8
PINATTR PinName C
PINATTR SpiceOrder 3
PIN -48 48 LEFT 8
PINATTR PinName N
PINATTR SpiceOrder 4
```